Thesis Summery:

Study on Shear Strength and Deformability Properties of Rock Masses by In-situ and Laboratory Testing Methods

By: Abbas Taheri

1. Introduction

In many countries, the number of construction works for large scale structures has increased recently, and stability-based designs are being replaced with displacement-based designs. Therefore, measuring stress-strain relationship of goematarials is very essential. Recent development in laboratory testing techniques has made it possible to evaluate the stress-strain relationships of geomaterials much more accurately than it was before. But, due to some engineering issues such as scale effect and quality of sampling, there are formidable difficulties in the sampling and testing of undisturbed samples that are sufficiently large to represent rock mass properties. This difficulty is significance in severely jointed rocks which are difficult to obtain large undisturbed samples and sedimentary soft rocks in which despite their uniform nature, sample disturbance is often a matter of question due to their weakness. Therefore, direct measurement of rock mass properties is found to be the most accurate and reliable method.

To study deformation properties of rock masses, large-scale field tests such as plate load test, flat jack test and pressuremeter test are very common in engineering projects. But, stress-strain relationships can not be measured directly and they are mostly suffering from loosening and disturbing effect. Apart from deformation characteristics, strength characteristics of rock masses have been investigated separately in general, by in-situ rock shear tests. But since the measurements are done on the predefined shear surface, field shear box test is most widely used for determination of discontinuity strength parameters (Tani, 1994). These inevitable problems in current in-situ rock mass testing methods, lead to the idea that, good site characterization and use of an appropriate rock mass classification method, give better results than in-situ measured results (Palmstrom et al., 2001). But, since the application of classification methods is mostly limited to the preliminary stages of the engineering projects, detail field testing methods can not be replaced by them.

To provide a solution to the above problems, down-hole large triaxial testing equipment was developed (Tani et al., 2003). A series of field tests were curried out in a tuffaceous rock in Japan. The testing apparatus successfully measured the direct relationships of stress and strain of the rock mass. In 2006, new trial series of tests were carried out at the site of rhyolitic tuffacious rock and rudaceous rock (Okada et al., 2006). The results were acceptable and it was generally agreeable with previous studies results in the same site. Nevertheless successful results being obtained by large in-situ triaxial apparatus, due to large specimen size and complicated measurement system, loading test in deep ground was expected to be too costly and impossible on practical level. So a need was arisen to develop a new small testing equipment to reduce testing costs and enhance applicability to deep rock mass.

In addition, there are some more issues associated with determination of mechanical properties of rock masses which deserve to be considered in this study.

Multiple-step Loading Triaxial Compression Test, hereafter denoted as ML-TCT, was proposed by Kovari and Tisa (1975). Since this new test method allows evaluation of strength parameters using only a single specimen, it is very useful for the case of non-homogeneous rocks or when the number of specimen is limited. However, the shear strengths are prone to be underestimated by ML-TCTs (Kim and Ko, 1979). Therefore, it is necessary to evaluate the applicability of this test method for various stress paths and types of rocks. In addition, any kind of modification in ML-TCT method in order to reduce the margin between results of obtained results with original results of conventional triaxial testing will be desirable and give more validity to this test method.

Moreover, in an effort to optimize the multiple-step testing procedure, various criteria for determining the axial load stopping point have been evaluated. Several researchers (Cain et al., 1986; Crawford and Wylie, 1987 & Pagoulatos, 2004) have used the volumetric strain as a criterion to determine stopping point of axial loading. But, it needs precise measurement of the axial and lateral deformation during testing, which is usually difficult. Another disadvantage is the necessity of re-setting the strain values for the next step of the test on a reference value of zero permanent strain, which may result in having more difficulty during testing and analyzing the data. In addition, the ISRM suggested method (Natau and Mutschler, 1989) has suggested to increase axial load until the axial stress-strain curve show a horizontal tangent (E_{tan}=0). However, due to large plastic deformations in the specimen immediately before arriving to this critical point, the shear strengths obtained by this method are seems to be underestimated comparing with those for intact specimens. Therefore, proposing a new method seems to be necessary.

Finally, in ML-TCT, it is assumed that the deformation characteristics should only be measured in the first loading step (JGS, 2001). However, the variations of stiffness in the following loading steps and the effect of confining pressure on stiffness have not been discussed in the literatures.

As a result, the overall objective of this thesis is to improve rock mass testing and characterization procedures. The study focused on both in-situ and laboratory testing method, new testing methods were developed and general knowledge of multiple-step loading triaxial compression testing was improved.

2. Down-Hole In-Situ Triaxial Testing Method

2.1. Developing an in-situ triaxial testing method

2.1.1. Apparatus

In this testing method, in order to measure the stress-strain relationship of deep rock masses directly in the field, a columnar specimen is supposed to be prepared and tested at the bottom of a borehole. So, direct access to the specimen is difficult to attach instrumentation devices and also to apply pressure and required loads. For this reason, a

unified apparatus is developed and equipped with all the facilities to apply confining pressures and axial loads and to monitor induced deformations of the rock specimen in deep ground without any need to access the specimen (Fig. 1). The apparatus consists of a triaxial cell and a separate axial loading system.

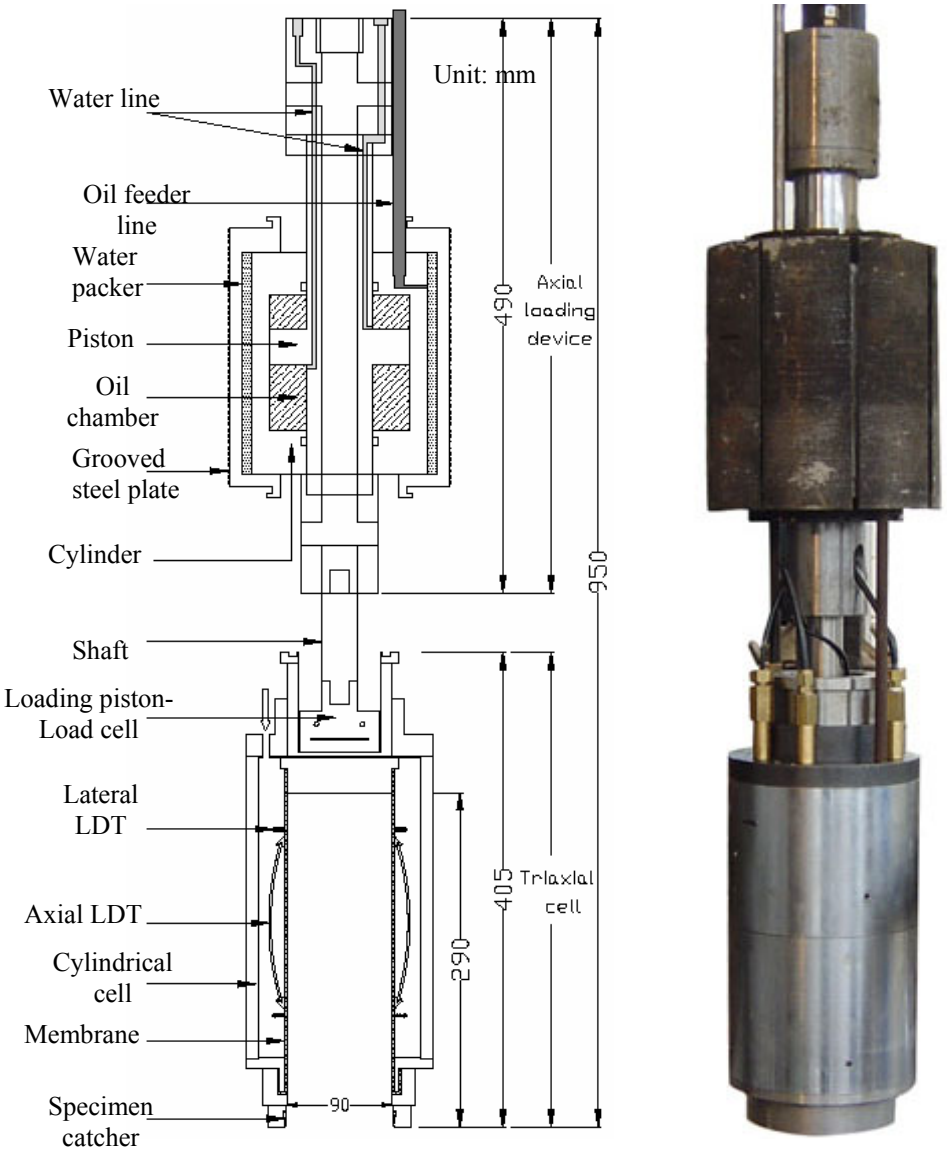

Fig. 1. Down hole triaxial testing apparatus

2.1.1.1 Axial loading system

A new loading system is developed which enables the apparatus to be used in any depth (Fig.1). The loading system mainly consists of 8 grooved steel plates which are placed around a cylindrical jack. A packer is located behind steel plates with a water line as feeder of the packer. In the middle of the apparatus is a cylindrical jack equipped with a piston, a central pipe and two oil lines.

The axial loading system is lowered to the bottom of the borehole with the triaxial cell, and the packer is filled and expanded by water before applying axial load. The water

pressure is increased to the desired level so that the grooved steel plates apply normal force to the borehole wall which provides the necessary reaction for the axial load. The axial load to the specimen is provided by a hydraulic jack consisting of a cylinder and a piston with two oil lines feeding hydraulic pressures to the upper and lower chambers. The upper chamber is firstly filled with oil and the axial load is applied to the loading shaft through the central steel pipe connected to the piston. After finishing the test, the lower chamber is filled with oil to let the piston push back to the previous state.

2.1.1.2. Triaxial cell

The greatest innovation in developing the triaxial cell is that all the measuring devices are placed inside the cell. A cylindrical specimen of rock prepared at the bottom of the borehole is encased in the triaxial cell subjected to a confining pressure, then loaded axially to failure while monitoring deformation of a specimen.

Fig. 1 shows the configuration of triaxial cell. A load cell on a rigid cap is placed to measure the axial forces. A rubber membrane provides enough protection against leakage. The instrumentation devices are installed on the membrane to measure displacements of the specimen. The named "Specimen catcher" is installed in the bottom ring to hold the bottom of the specimen for retrieving after finishing the test.

2.1.1.3. Confining pressure

Confining pressure is applied to the specimen using a hydraulic pump capable of applying 2.5 MPa pressure. A pressure transducer is placed at ground surface to measure the confining pressure.

2.1.1.4. Measurement of deformations

As shown in Fig. 1, a pair of axial and lateral LDTs is used to measure axial and radial deformations of the specimen. The axial LDT is a type of clip gage and consists of a phosphor bronze strip that is attached to the membrane at the mid-height and on the lateral surface of specimen at the opposite sides diametrically. A set of electric-resistant strain gages consisting of a Wheastone bridge is attached to both sides of the central part of the strip to detect the axial deformation of specimen very accurately. Lateral ring-shape LDTs are placed next to the axial LDT near to the end of the membrane.

2.1.2. Drilling and preparation of the specimen

A conventional rotary drilling machine is used for drilling and preparation of the specimen. As shown in Fig. 2, drilling and preparation of the specimen has 3 stages as follows:

1. Using a diamond drilling bit of diameter 200 mm, the borehole is drilled before the top of the specimen (Fig. 2a).
2. With a diamond drilling bit of diameter 160 mm another 50 mm is drilled. The area prepared by drilling accommodates the cylindrical triaxial cell to fix during testing without any play. The bottom flat surface of the drill hole will serve as the top of the specimen (Fig. 2b).
3. To prepare a cylindrical specimen of diameter 90 mm and height 285 mm, at the bottom of the drill hole, (Fig. 2c), a special core barrel with drilling bit is used.

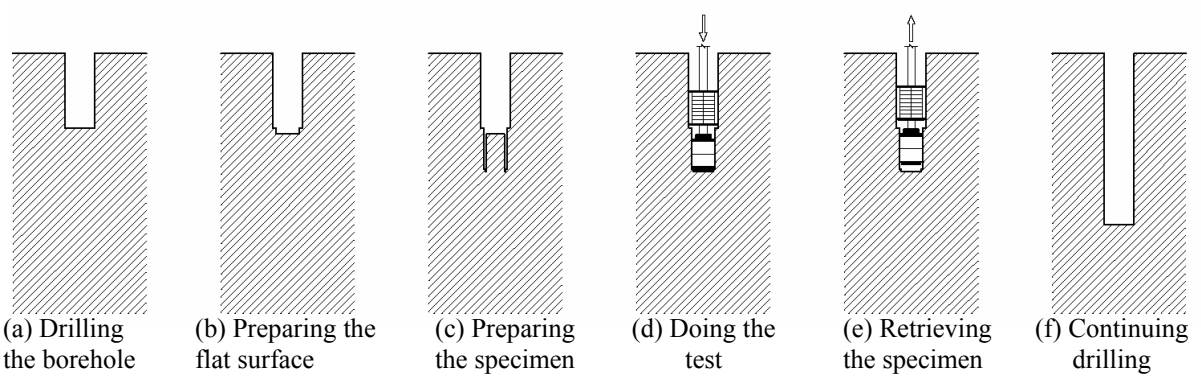

Fig. 2. Testing procedure of down-hole triaxial test

2.1.3. Testing procedure

The testing procedure is as follows (Fig. 2):

(a) Set the instrumentation tools to the membrane, assemble the cell, and connect it to the axial loading system;

(b) Lower the apparatus into the borehole and let the specimen to be encased by the cell;

(c) Apply hydraulic pressure to the packer inside axial loading system to provide the necessary reaction force to apply axial load;

(d) Increase the axial load and the cell pressure simultaneously up to the predetermined level for the confining pressure is reached;

(e) Apply the axial load of desired magnitude and strain rate to the specimen; (Fig. 2d)

(f) Record the stress and strain histories, together with pressure measurements, continuously by the data recording system;

(g) Cut the specimen at its bottom and lifted the apparatus with specimen to the ground surface for further observation; (Fig. 2e);

(h) Continue drilling for future tests (Fig. 2f).

2.2. Down-hole in-situ triaxial testing

In Sagamihara city of Japan, a 50 m deep large-diameter cavern at the bottom of a shaft were excavated for research purpose in a sedimentary soft rock, mudstone. This research site was selected to test the new down-hole triaxial testing apparatus. Using the new developed apparatus, a series of field down-hole triaxial tests (DHTT) were carried out in several depths with different loading methods.

For in-situ tests, a borehole was excavated in the cavern and three specimens were prepared at the bottom of the borehole. ML-TCT method was selected to determine Mohr-Coulomb's failure envelope in each specimen in a series of consolidation and shearing stages. Multiple-step loading was conducted in five steps of confining pressures, 0.4, 0.8, 1.2, 1.6 & 2.0 MPa.

2.2.1. Test results

2.2.1.1. Stress and strain relationship

Fig. 3 shows the relationships between the deviatoric stress, q = axial stress, σ_a, - confining stress, σ_c, and the axial, ε_a, and lateral, ε_r, strains for the first step of loading in

Test 3 as a typical result. The axial strains, ε_a, are calculated in two ways; the local strains are calculated as average values of two LDTs installed on the opposite sides of the rubber membrane diametrically, and the external strains are recorded by the external LVDT which measures the axial movement of loading piston. Where circumferential strains, ε_r, are calculated as average radial strains measured by lateral LDTs at top and bottom of the specimen.

The presented results demonstrate that the proposed small down-hole triaxial testing method is successful in obtaining continuous curves of average stress-strain relationships of the rock masses. The amount of deformation measured by external LVDT is higher than the values recorded by local deformation transducer. This is because of bedding errors and also other deformations in loading piston, cap and axial loading system which recorded totally as the deformation of rock mass by external measurement device.

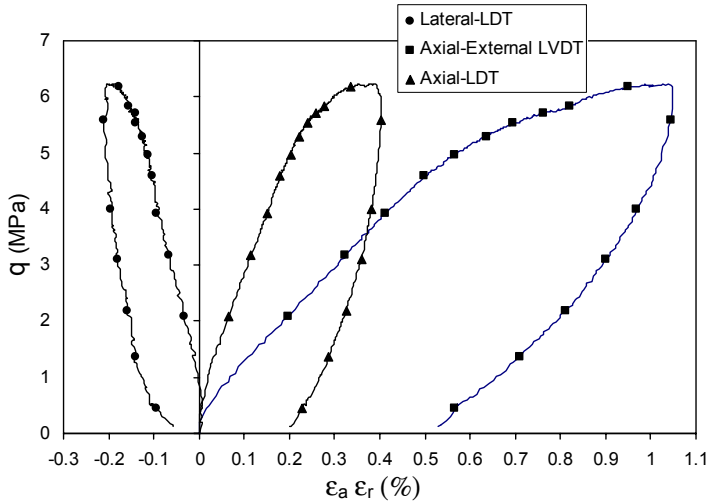

Fig. 3. example of stress-strain relationship in DHTT

2.2.1.2. Strength and deformation characteristics

Fig. 4 shows the Mohr-Coulomb's failure envelopes obtained by multiple-step loading tests. In Test 1, the failure of the specimen for each loading step was judged by the first detection of the decrease of axial load, i.e. strain softening. But due to the ductile behavior of mudstone, considerable displacement was induced at and close to failure point without any drop in the axial stress. This phenomenon caused excessive damage to the specimen for the following loading steps with higher confining pressures. The low value for friction angle (ϕ = 5 degree) and high value for cohesion (c = 2.51 MPa) could be attributed to this problem. Consequently, in the following tests, the axial stress was increased until the axial stress-axial strain curve shows a horizontal tangent, aiming for determination of peak strength without causing marked damage to the specimen in each loading step.

Due to existence of a sand layer in the middle of the specimen for Test 2, the multiple-step loading was not successful. The Mohr-Coulomb's failure criterion parameters are found by a best fit line as ϕ = 8 degree and c = 0.89 MPa.

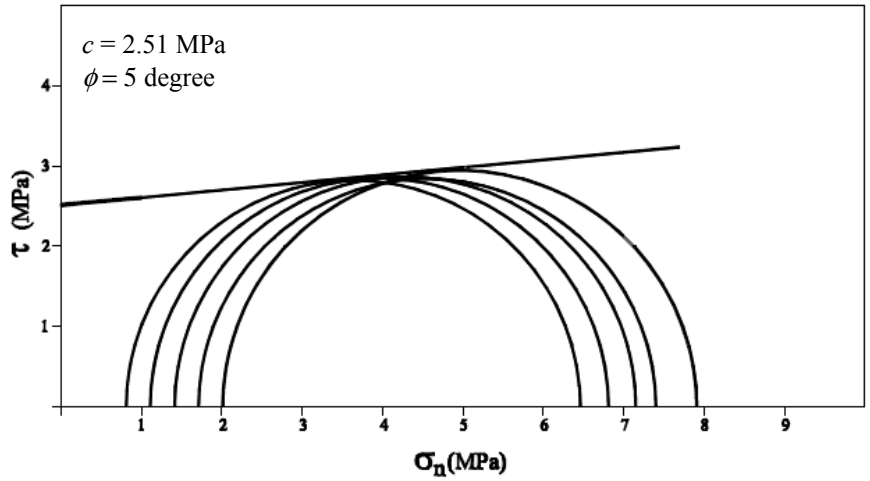

a) Test 1

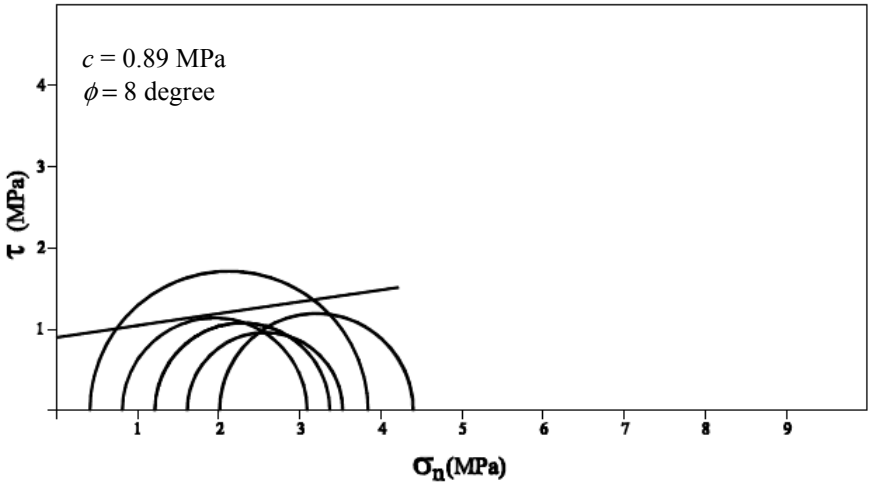

b) Test 2

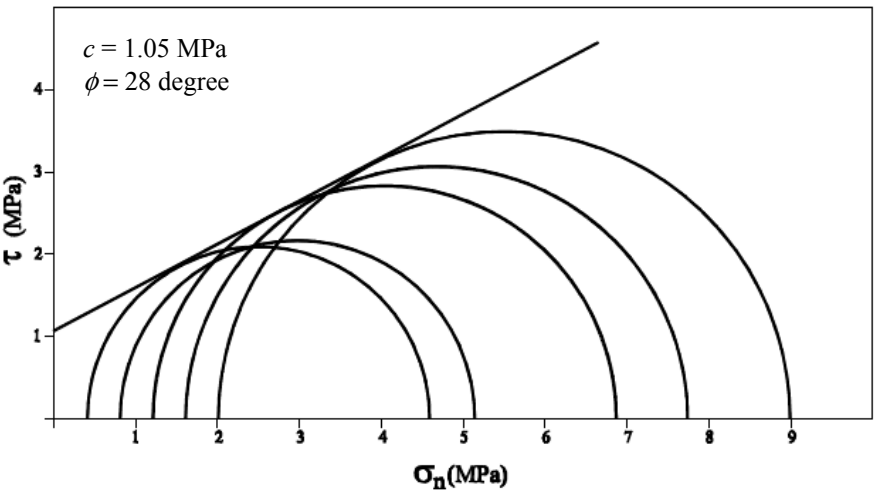

c) Test 3

Fig. 4. Mohr-Coulomb's failure envelop obtained from multiple-step loading tests

In Test 3, similar to the previous test, a sand layer reduced the strength in the first and the second steps of loading. But from the third step, apparent compression of the bottom of the specimen seems to be prevented by the steel ring at the bottom of the cell; and since then, the middle of the specimen seems to have failed. The result shows higher ultimate axial stresses in the last three loading steps. This demonstrates that, the multiple-step loading was successful in Test 3 with the shear strength parameters being as $\phi = 28$ degree and $c = 1.05$ MPa.

The obtained results show that, because of accumulative damage in the mudstone specimens with repeated cycles of axial loading/unloading, the shear strengths might be underestimated. Furthermore, in the second specimen, sand layer seems to have a far greater weakening effect during multiple-step loading. However, it would be too premature based on limited data at this time to propose a suitable loading method, loading path and method for determining of peak strength for this particular material.

Fig. 5 demonstrates the relationships of secant, E_{sec}, and tangent, E_{tan}, Young's modulus versus shear stress ratio, q/q_f, in Test 1, where q_f denotes the deviator stress at the peak state. These Young's moduli were calculated from measured axial strains using both axial LDT and external LVDT. The continuous degradation of E_{sec} and E_{tan} with shear deformations can be clearly seen. In Fig. 10, E_{sec} for LDT at the beginning of shear process q/q_f = 0 - 0.4 are significantly higher than that for external LVDT. The same trend is followed for E_{tan} up to q/q_f = 0.2. This inconsistency could be attributed to bedding errors and apparatus deformations measured by the external LVDT.

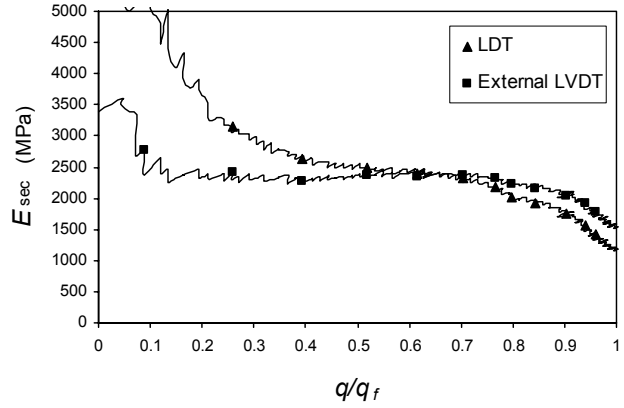

a) Secant Young's modulus

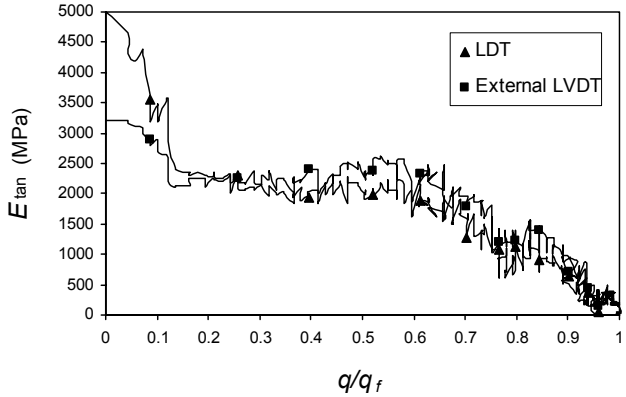

b) Tangent Young's modulus

Fig. 5. Deformation characteristics by Test 1 for 1st step

It is worth noting that, the continuous nature of the specimen's bottom to the ground inevitably prohibits drainage control to the boundary and applying back pressure similar to laboratory tests. The exact drainage condition within the test specimen under shear process cannot be known anyhow. However, by doing the test in saturated specimen, some information about drainage condition of the specimen is obtainable using results of lateral measuring device. Moreover, in the previous studies, results of CU and CD triaxial compression tests on the drilled cores revealed that, the mechanical properties of mudstone is almost independent of drainage condition during testing (Tatsuoka et al, 2003).

2.3. Verification of down-hole triaxial testing

To verify the results of down-hole triaxial testing, the obtained results were compared with those by traditional laboratory tests and field measurements in the same site.

2.3.1. In-situ measurement and testing methods

In Fig. 6, a comparison between various field testing methods, full-scale monitoring results and DHTT method is provided. The lateral displacement of the vertical shaft and the deformation in the ground surrounding the tunnel were carefully monitored by inclinometers installed behind the shaft wall and the Young's moduli, $E_{(\text{monitoring})}$, were back calculated. E_f was obtained from field shear wave velocity measurements. $E_{PMT(1)}$ and $E_{PMT(2)}$ were obtained from pre-bored pressuremeter tests, using so-called Menard's pressuremeter and Elastometer, respectively, whereas $E_{PMT(3)}$ was calculated using self-bored pressuremeter equipment. E_{PLT} was obtained from plate loading tests performed in the adits while measuring strains in the ground. Assuming the Poisson's ratio, $\upsilon = 0.3$, the values of $E_{PMT(1)}$, $E_{PMT(2)}$ and E_{PLT} were calculated from the loading curves, while the values of $E_{PMT(3)}$ were from small unload – reload loops. In addition, E_{DHTT} is E_{sec} determined at axial strain level of 10^{-3} from the first step of loading curve by axial LDT.

Fig. 6 shows that, different values are obtained by various testing methods. Among them, $E_{PMT(1)}$ and $E_{PMT(2)}$ are too small and not reliable comparing with those by the other testing methods. The discrepancy of the E_{DHTT} values from the $E_{PMT(1)-(3)}$ and E_{PLT} values could be due to the following reasons:

1. Errors due to loosening and disturbance in $E_{PMT(1)}$, $E_{PMT(2)}$ and E_{PLT} measurements.
2. Errors in $E_{PMT(1)}$ and $E_{PMT(2)}$ and $E_{PMT(3)}$ due to non-uniform deformation of borehole walls,
3. Sand layers,
4. Different measurement scale in different testing methods,
5. Different strain level in different testing methods.

2.3.2. Laboratory testing methods

Large amounts of unconfined and triaxial compression tests mostly undrained and partly drained were performed.

In Fig. 7, a comparison of Young's moduli (E) between laboratory triaxial testing methods and DHTT is presented. E_i is E_{tan} of a linear part of stress-strain curve using externally measured strains, whereas E_{max} is E_{sec} at small strains measured by LDT. In addition, E_d was calculated from ultra-sonic wave measurements in the laboratory using the drilled cores. These results clearly show that external axial strain measurements greatly underestimate the stiffness at small strains. Moreover, in Test 2 because of existence of a

sand layer in the middle of the specimen, the stiffness is reduced dramatically. But the stiffness values, E_{max} and E_{DHTT}, which were measured locally by LDT in laboratory tests and DHTT, are consistent and also are virtually the same as the E_d values obtained by laboratory ultra-sonic wave measurements.

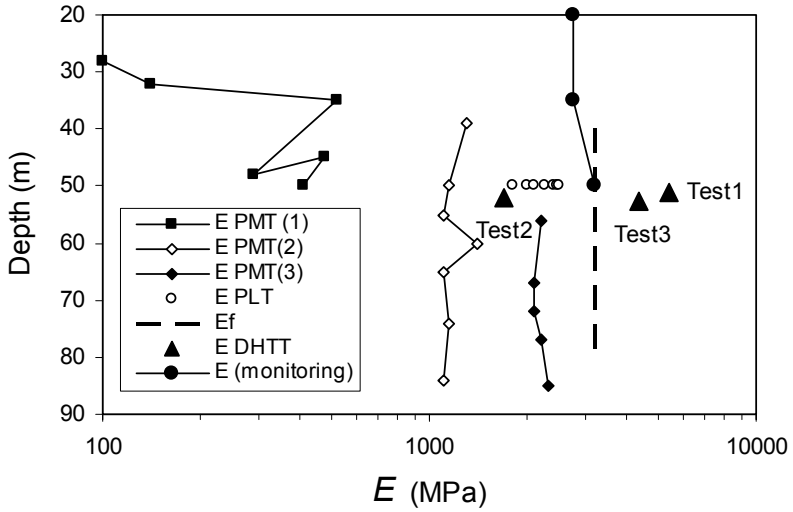

Fig. 6. Distribution of young's modulus by different field measurements (Strain level equal to 10^{-3} in E_{DHTT})

A comparison of DHTT and laboratory unconfined and triaxial compression tests is given in Fig. 8, as a relationship between compression strength versus confining pressure. Due to a sand layer, low strength values are exhibited for Test 2. In Test 3, similar to the previous test, a sand layer reduced the measured strengths in the first and second steps of loading. Therefore, the results of Test 1 and Test 3 after third loading step are agreeable with laboratory test results with respect to the confining pressure level.

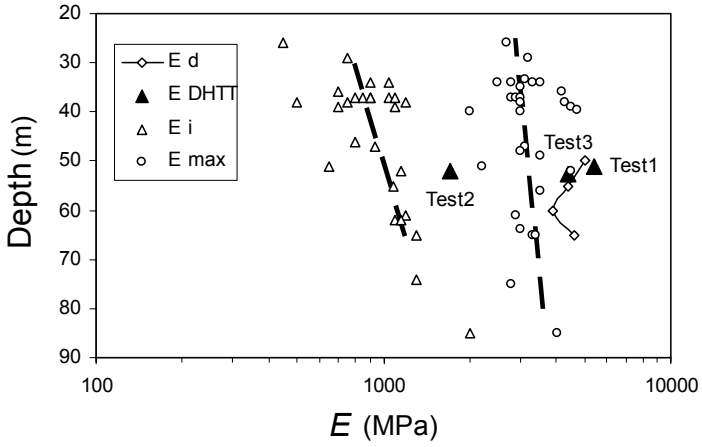

Fig. 7. Distribution of Young's modulus for small strains by DHTT method and laboratory testing methods

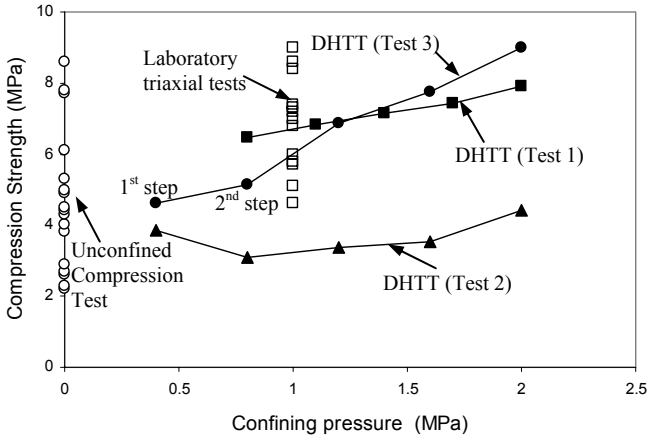

Fig. 8. Strength of mudstone by DHTT and laboratory testing methods

3. Study on multiple-step loading triaxial testing method

3.1. Triaxial compression testing

To carry out the study, a laboratory triaxial compression testing system was used. Axial strains were measured both externally and locally by means of a pair of proximeters. Core samples of sedimentary mudstone were retrieved from two boreholes in an adit excavated in Sagamihara experimental cavern. Total numbers of 18 triaxial compression testing were carried out.

Two series of Multiple-step Loading Triaxial Compression Tests (ML-TCT) were conducted. The first series was carried out to determine all the geotechnical parameters to describe the MLD model for the relevant rock, where repeated cycles of axial loading/unloading were made under the same confining pressure. Moreover, the second series was carried out to verify the MLD model, where repeated cycles of axial loading/unloading were made under different confining pressures.

3.2. Stiffness variations during multiple-step loading

The effects of confining pressure and accumulated damages in the specimen during shearing on the stiffness were studied.

In each loading step, the results were compared to study the variation of stiffness at small strain level ($0<q/q_f<0.1$) and in four other shearing stages. The comparison showed that in ML-TCTs, regardless of the chosen confining pressure, the stiffness of mudstone specimens in the first loading step during shearing found to be the highest value. The obtained results from this loading step at small strain level, $\varepsilon_a<10^{-5}$, were also in good agreement with those measured by ultrasonic wave measurements. In addition, the stiffness was influenced both by accumulated damages to the specimen and confining pressures. These effects were compensated by each other in increasing manner test and added to each other in decreasing manner test.

3.3. Stress path and judgment of ultimate deviator stress

It is aimed to design a ML-TCT method, that could be followed smoothly and easily to yield a failure envelope from a single specimen comparable to the one obtained using the conventional technique. The approach is focused on two fundamental issues; first where the axial loading should be stopped for each loading stage; and second what loading path should be followed.

In this study, the axial load reversal point was evaluated at each confining pressure based on secant Young's modulus curve measured by external measurement device. This method is proposed to avoid partial or total failure of the specimen. During ML-TCT, the secant stiffness keeps increasing; the "Sigh of failure" is defined as the plateau of the secant stiffness – axial strain plot after leaving the elastic region before E_{sec} starts decreasing.

In Fig. 9, the author's suggested method and the ISRM suggested method are compared by plotting axial stress –axial strain and secant stiffness – axial strain curves. As it is shown, the point where stress increments become smaller marks the beginning of the stress state where the specimen has unstable failure propagation. This point is recognized as the point where secant stiffness becomes a pick (E_{sec}=max). The procedure used to perform the modified ML-TCTs is described briefly as follows:

1. The strain readings are set to zero. The axial load, Q, and the confining pressure, σ_c, are increased simultaneously for the isotropic confining pressure.
2. The axial load, Q, is increased continuously under displacement control keeping the confining pressure, $\sigma_{c,1}$, constant. Axial strain is recorded and secant stiffness is calculated and plotted using external measurement device.
3. Loading is stopped once secant stiffness, E_{sec}, becomes constant and starts to decrease. The axial load, Q, is slowly reduced to the isotropic stress state.
4. The axial load, Q, and the confining pressure, σ_c, are then increased simultaneously for the isotropic confining pressure of the second step. This is followed by an axial loading and unloading using the procedure described in 2&3.
5. The stepwise procedure described in 2-4 is repeated until the peak strength for the last step is reached.

Two series of ML-TCTs were carried out in increasing and decreasing confining pressure steps. In the first series the failure of the specimen for each loading step was judged by detecting a plateau in the axial stress – axial strain curve (E_{tan}=0). Whereas, in the second series observing a plateau in the secant stiffness – axial strain curve was considered as a criterion to reverse axial load (E_{sec}=max). For each testing method two tests were done in increasing manner and one test in decreasing manner.

The main goal of the multiple-step test is to give results comparable to those obtained conventionally with the existing expensive and time consuming methods. For this, specimens that were characterized and found to be homogeneous were used to construct a references failure envelope for comparison of the results of the modified method. The Mohr-Coulomb's shear strength parameters were used to define the accuracy of the modified method.

Table 1 which is related to Mohr-coulomb shear strength parameters in terms of effective stresses, present the results of a comparison between ISRM, E_{tan}=0, and modified, E_{sec}=max, methods. It may be seen from the table that using the modified method,

E_{sec}=max, the amount of differences in cohesion, c, and friction angle, ϕ, between SL-TCT and ML-TCT are greatly reduced and the results obtained by the modified method are comparable with those obtained by conventional single-step test.

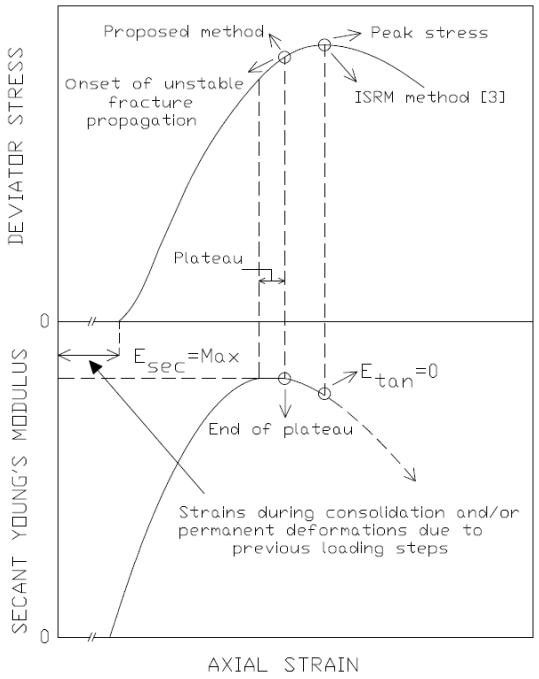

Fig. 9. Stress – strain and secant stiffness – strain relations in rock during shearing

Therefore, it is found that, the proposed method can guarantee the integrity of the specimen with minimum alteration of its mechanical properties, as excessive plastic deformation can be avoided. Moreover, the method is not confining pressure dependent and the load reversal point can be easily identified by using the data of an external deformation measurement device. The most important point is that, this method could give results that are comparable to the values obtained by the conventional multiple sample method. It can minimize errors due to operator subjectivity and is an easy and repeatable procedure.

Table 1. Comparison between different loading paths in multiple-step loading methods

Loading method	**c' (MPa)**	**ϕ' (Deg)**	**Differences in (c') values (MPa)**	**Differences in (ϕ') values (Deg)**	**Error (c') %**	**Error (ϕ') %**
SL	1.47	34.3	-	-	-	-
ML- Increasing E_{tan} = 0 (1)	2.08	20.8	0.61	-13.5	41.5	-39.4
ML- Increasing E_{tan} = 0 (2)	2.38	13.1	0.90	-21.2	61.4	-61.7
ML- Decreasing- E_{tan} = 0	0.53	42.0	-0.94	7.8	-63.7	22.6
ML- Increasing- E_{sec} = max (1)	1.69	26.1	0.21	-8.2	14.5	-23.8
ML- Increasing- E_{sec} = max (2)	1.59	36.6	0.12	2.4	8.0	6.9
ML- Decreasing- E_{sec} = max	1.68	25.5	0.20	-8.7	13.8	-25.5

3.4. Proposal of a multiple-step loading damage model

3.4.1. Concept of multiple-step loading damage model, MLD model

Fig. 10 schematically demonstrates the results of a ML-TCT conducted to determine the geotechnical parameters to describe the MLD model. The relationships between the deviator stress, q, as well as the excess pore water pressure, Δu, and the axial strain, ε_a, are shown for repeated cycles of axial loading/unloading under the undrained condition and isotropic consolidation under the constant effective stress, σ'_c. The residual axial strain after the isotropic consolidation following the i-th cycle of axial loading/unloading is denoted as the cumulative plastic axial strain, ${\varepsilon_a}^p{}_i$. In the proposed MLD model, this ${\varepsilon_a}^p{}_i$ is assumed to represent the amount of damage accumulated in the specimen during the previous cycles of axial loading/unloading.

Fig. 11 schematically demonstrates the five relationships to formulate the MLD model. The shear strength and the excess pore water pressure at failure for Single-step Loading Triaxial Compression Test (SL-TCT), $q_{f,SL}$ and $\Delta u_{f,SL}$, can be measured from the first loading step of ML-TCTs. Thus, the $q_{f,SL}$ - σ'_c relation, Fig. 11(a), and the $\Delta u_{f,SL}$ - σ'_c relation, Fig. 11(b), are evaluated from ML-TCTs conducted under different values of σ'_c. From the second and the following loading steps of ML-TCTs, the shear strength ratios, $q_{f,ML,i}/q_{f,SL}$, and the excess pore water pressure ratios, $\Delta u_{f,MLi}/\Delta u_{f,SL}$, can be evaluated where $q_{f,ML,i}$ and $\Delta u_{f,MLi}$ are the shear strength and the excess pore water pressure at failure for the i-th loading step of ML-TCTs. As shown in Figs. 11(c) & 2(d), these two ratios are assumed to be expressed as the functions of the cumulative plastic axial strains at the previous, i.e. (i-1)-th, loading step, ${\varepsilon_a}^p{}_{i-1}$, and σ'_c. Furthermore, the increment of plastic axial strain for the i-th loading step, $\Delta{\varepsilon_a}^p{}_i = {\varepsilon_a}^p{}_i - {\varepsilon_a}^p{}_{i-1}$, is also assumed to be given as the function of ${\varepsilon_a}^p{}_{i-1}$ and σ'_c as shown in Fig. 11(e).

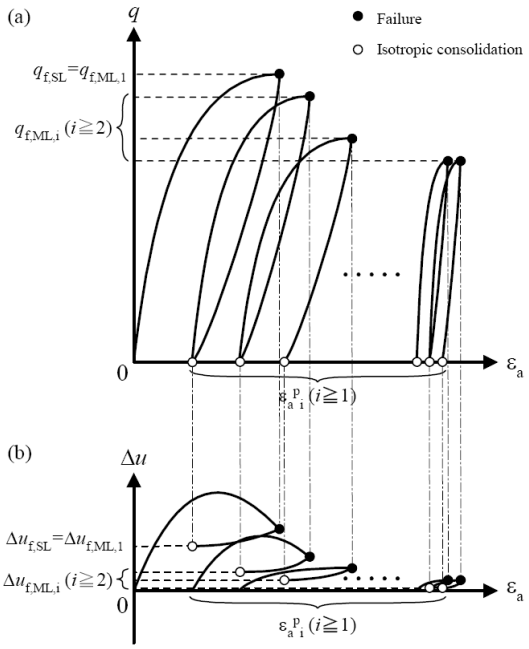

Fig. 10. Definition of geotechnical parameters obtained from ML-TCT to describe MLD model

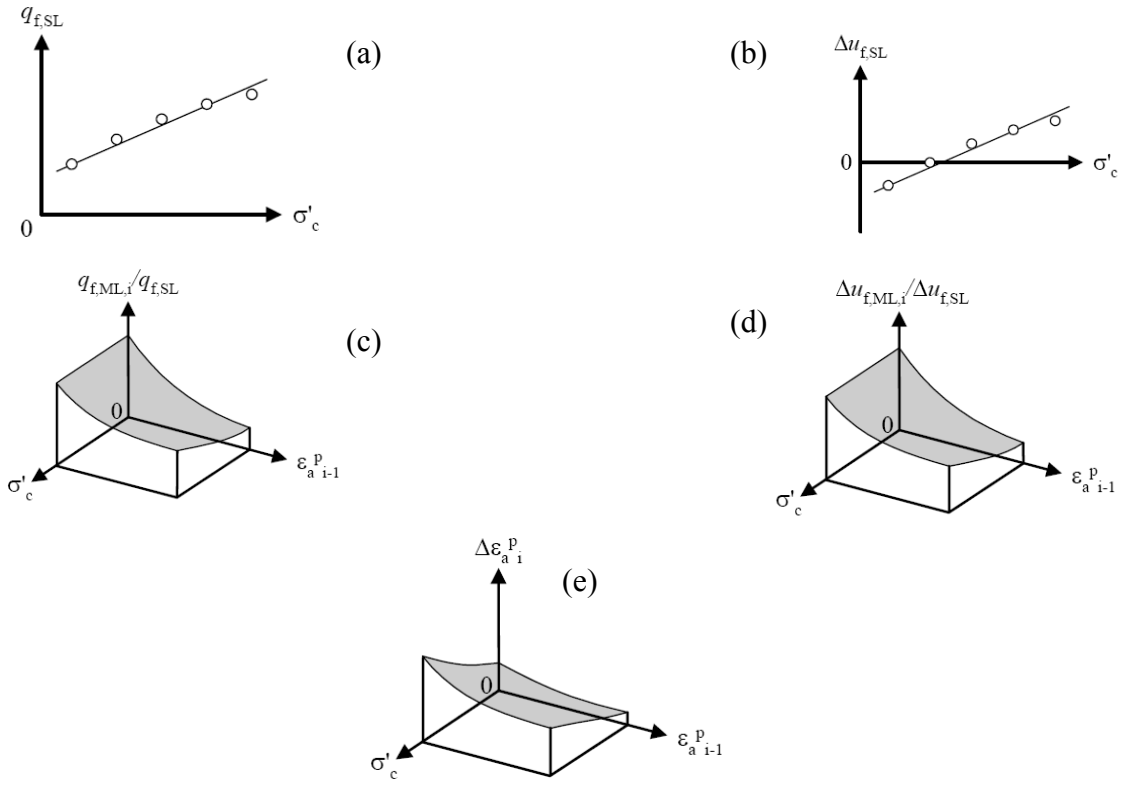

Fig. 11. Concept of MLD model

3.4.2. MLD model for mudstone

A MLD model was developed to simulate ML-TCTs on the mudstone with various stress paths. This model is comprised of five relationships as schematically demonstrated in Fig. 2, and was prepared on the basis of the results obtained from the first series of ML-TCTs.

In 2007, the author developed another MLD model to simulate ML-TCTs on a siltstone (q_u= 3-4 MPa). The results from both studies were used towards understanding of the changing trend of $q_{f,ML,i}/q_{f,SL}$, $\Delta u_{f,MLi}/\Delta u_{f,SL}$ and $\Delta\varepsilon_a{}^p{}_i$ with $\varepsilon_a{}^p{}_{i-1}$. As a result, in Fig. 12, the MLD model which was developed for mudstone is simplified to describe the above stated observations and findings by some smooth curves. This simplified model allows prediction of peak deviator stress and the relevant excess pore pressure of the mudstone for each axial loading/unloading step.

3.4.3. Verification of MLD model

The verification was made using two following approaches. Firstly, comparisons were made between the experimental results of the second series of ML-TCTs and the calculated results of the MLD model with the identical stress path. The calculated results were mostly agreeable with the experimental results for both stress paths with increasing and decreasing values of σ'_c.

In addition, attempts were made to modify the results of second series of ML-TCTs based on the MLD model and to compare the modified results with results of SL-TCTs. It was observed that using the MLD model, the amount of differences in cohesion, c', and

friction angle, ϕ', between SL-TCT and ML-TCT are greatly reduced and the results which were modified by the MLD model are comparable with those obtained by conventional single-step loading tests.

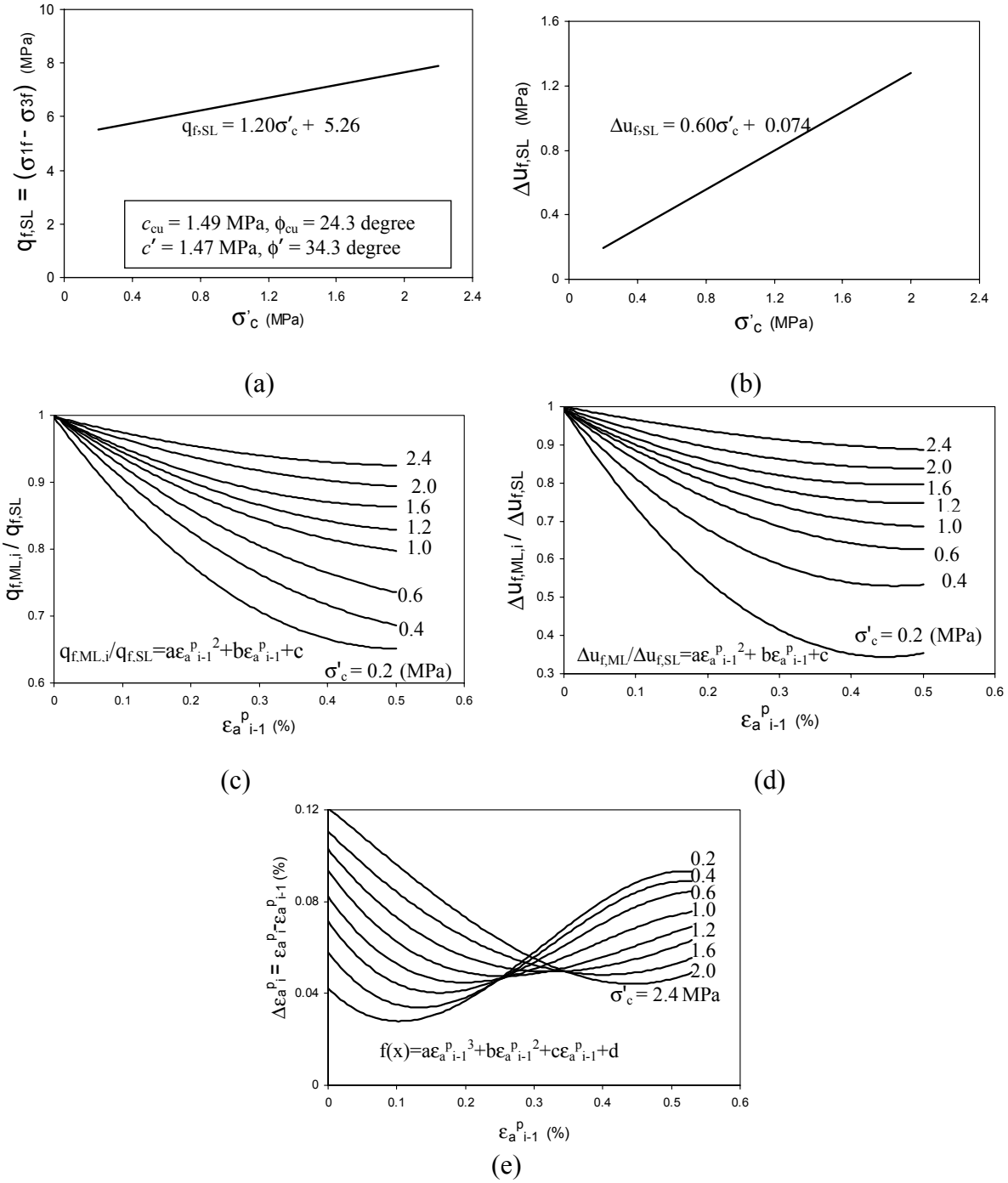

Fig. 12. Simplified MLD model for the mudstone

3.4.4. Generalized MLD model for rocks

Having established MLD models for mudstone and siltstone, attempt was made to extend the MLD model to all types of rock. Therefore, based on these two models and considering the stress-strain behavior of different types of rock from start of shearing up to the post failure a generalized MLD model is proposed.

To verify the generalized MLD model, comparison were made between the experimental results of second series of ML-TCTs on the mudstone of q_u=6-8 MPa, and the calculated results of the ML-TCTs with the identical stress path. It was found that, the calculated results are agreeable with the experimental results for both stress paths with increasing and decreasing values of σ'_c.

To verify the model for other types of rock, a numerical simulation was carried out to predict ML-TCT in three typical soft, medium-hard and hard rock. Two ML-TCTs were simulated in increasing and decreasing manner under the different confining pressures.

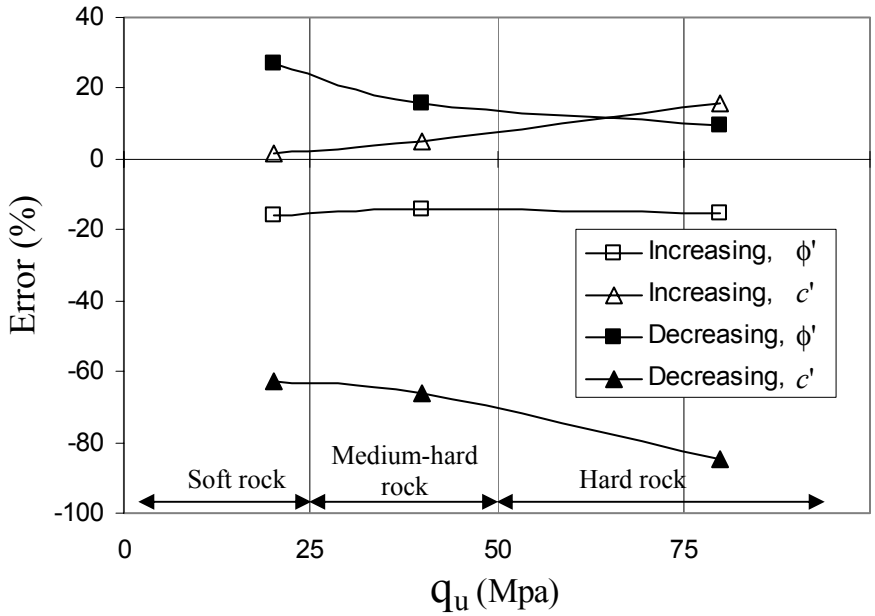

Fig. 13. Results of simulation of ML-TCT by MLD model in different types of rock and loading path

The results are compared in Fig.13 based on the error in each type of rock and loading method for Mohr-Coulomb shear strength parameters. The upper bound values for c' and lower bound values for ϕ' could be resulted from ML-TCT with increasing confining pressure steps, whereas, an opposite trend can be seen for ML-TCTs with decreasing confining pressure steps. As can be seen, in increasing manner test, the amount of error for cohesion, c', increases with rock strength, whereas for friction angle, ϕ', seems to be constant with rock strength increase. Whereas, in decreasing manner test, with rock strength increase, the margin between results of single-step loading test and multiple-step loading test decrease for friction angle, ϕ', and increase for cohesion, c'. Moreover, since, the difference between amounts of effective cohesions obtained by single-step loading test and decreasing multiple-step loading test is significantly large, ML-TCTs with increasing

confining pressure steps is preferable to those with decreasing confining pressure steps for all types of rock.

Finally, attempt was made to compare the results of DHTT with those obtained by laboratory testing. For this, the results of DHTT which were done by ML-TCT were modified using MLD model. The comparison showed that the results of traditional laboratory triaxial testing and DHTT are comparable and MLD model was also successful in modifying the results of ML-TCT obtained by DHTT and producing more reliable values.

4. Conclusions

The following conclusions are drawn:

1. To solve the problem of sampling disturbance in soft rocks, a new testing method is introduced to measure the shear strength and stiffness of the rock mass directly in the field. A down-hole triaxial testing apparatus is developed and a special procedure for drilling and preparation of the specimen was presented.
2. The proposed small down-hole triaxial testing method was successful in obtaining continuous curves of average stress-strain relationships of the rock masses in depth.
3. The comparison between results of DHTT and traditional field and laboratory testing methods shows that the new testing method is free of sampling disturbance and some inherent errors associated with other testing methods. Therefore it seems that, DHTT method is a reliable tool to measure shear strength and deformability properties of soft rocks for which the effect of discontinuities are not obvious.
4. In ML-TCTs, the stiffness was influenced both by accumulated damages to the specimen and confining pressures. These effects were compensated by each other in increasing manner test and added to each other in decreasing manner test.
5. A new approach for defining the stopping point of axial load increase and loading path in ML-TCT is proposed. The axial load reversing point is defined as the plateau of the secant stiffness – axial strain plot after leaving the elastic region before starts decreasing (E_{sec} =max, method). The results obtained by this modified method are comparable with those obtained by conventional single-step test.
6. For the purpose to investigate the applicability of multiple-step loading triaxial compression tests, ML-TCTs, multiple-step loading damage model, MLD model, was proposed to simulate ML-TCTs with various stress paths. In MLD model, the damage accumulated in the specimen by the repeated cycles of axial loading/unloading is represented by the plastic axial strains. The verification of the MLD model was made using two approaches. In addition a unified MLD model was constructed for all types of rock. The unified model was verified using experimental results and numerical simulations.
7. Comparison between laboratory SL-TCT results and those obtained by DHTT showed that the results are comparable and MLD model is also successful in modifying the results of ML-TCT obtained by DHTT and produce more reliable values.

References

[1] Cain, P., Yuen, G. Lebel, Crawford, A. and Lau, D. (1986): Triaxial testing of brittle sandstone using a multiple failure state method. Energy, Mines and Resources, Canada – CANMET, Energy Research Progrom, Coal Research Laboratories, Division Report ERP/CRL 86-104.
[2] Crawford, A. and Wylie, D. (1987): A modified multiple failure state triaxial testing method, *Proc. of 28th US Sym. on Rock Mechanics*, 133-140.
[3] JGS (2001): Triaxial compression test on soft rock, Jap. Geotech. Standard, JGS 2533-2001.
[4] Kim, M.M. and Ko, H.Y. (1979), Multistage triaxial testing of rocks, *Geotechnical Testing Journal*, **2**, 98-105.
[5] Kovari, K. and Tisa, A. (1975): Multiple failure state and strain controlled triaxial tests, *Rock Mechanics*, **7**, 17-33.
[6] Natau, O.P. and Mutschler, T.O. (1989): Suggested method for large scale sampling and triaxial testing of jointed rock, *Int. J. Rock Mech. & Min. Sci.*, **26** (5), 427–434.
[7] Okada, T., Tani, K., Ootsu, H., Toyooka, Y., Hosono, T., Tsujino, T., Kimura, H., Naya, T. and Kaneko, S. (2006): Development of In-situ triaxial test for rock masses. *Int. J. JCRM*, **2** (1), 7-12.
[8] Pagoulatos, A. (2004): Evaluation of multistage triaxial testing on Berea sandstone, *MSc dissertation*, The University of Oklahama.
[9] Palmstrom, A. and Singh, R. (2001): The deformation modulus of rock masses - comparisons between in situ tests and indirect estimates, *Tunneling and Underground Space Technology*, **16** (3), 115–131.
[10] Tani, K. (1994): General Report: Measurement of shear deformation of geomaterials – Field tests, *Proc. of 2nd Int. Sym. on Prefailure Deformation of Geomaterial,* Vol 2, 1115-1131.
[11] Tani, K., Nozaki, T., Kaneko, S., Toyo-oka, Y. and Tachikawa, H. (2003): Down-hole triaxial test to measure average stress-strain relationship of rock mass, *Soils and Foundations*, **43** (5), 53-62
[12] Tatsuoka, F., Hayano, K. and Koseki, J. (2003): Strength and deformation characteristics of sedimentary soft rock in the Tokyo metropolitan area, *Proc. of Characterization and Engineering Properties of Natural Soils*, Swets and Zeitlinger, 1461-1525.